

Mn Diffusion and Reactive Diffusion in Ge: Spintronic Applications

Alain Portavoce^{1,a*}, Omar Abbes^{2,b}, Sylvain Bertaina^{1,c}, Yauheni Rudzevich^{3,d},
Lee Chow^{3,e}, Vinh Le Thanh^{4,f}, Christophe Girardeaux^{2,g} and Lisa Michez^{4,h}

¹CNRS, IM2NP, Faculté des Sciences de Saint-Jérôme case 142, 13397 Marseille, France

²Aix-Marseille Université, IM2NP, Faculté des Sciences de Saint-Jérôme case 142, 13397
Marseille, France

³Department of Physics, University of Central Florida, Orlando, FL 32816, USA

⁴Aix-Marseille University, CINAM, Campus de Luminy case 913, 13288 Marseille, France

^aalain.portavoce@im2np.fr, ^bomar.abbes@im2np.fr, ^csylvain.bertaina@im2np.fr,

^dyauheni.rudzevich@ucf.edu, ^elee.chow@ucf.edu, ^flethanh@cinam.univ-mrs.fr,

^gchristophe.girardeaux@im2np.fr, ^hmichez@cinam.univ-mrs.fr

Keywords: Germanium, Manganese, Diffusion, Reactive-diffusion, spintronics.

Abstract. In this paper, we report investigations concerning the fabrication of a diluted Ge(Mn) solution using solid state Mn diffusion, and Mn/Ge reactive diffusion for spintronic applications. The study of Mn diffusion shows that the quasi-totality of the incorporated Mn atoms occupies Ge substitutional sites and probably exhibits two negative elementary charges. The solubility limit of Mn in Ge is comprised between 0.7 and 0.9 % ($T \leq 600$ °C). We show that substitutional Mn atoms are not ferromagnetic in Ge and consequently that Ge(Mn) diluted magnetic semiconductor can not be produced. Beside the ferromagnetic signal from Mn₅Ge₃, ferromagnetic signals detected in the samples could be always attributed to surface or bulk Mn-Ge clusters. Furthermore, we show that the CMOS Salicide process is potentially applicable to Mn₅Ge₃ nano-layer fabrication on Ge for spintronic applications. During Mn(thin-film)/Ge reaction, Mn₅Ge₃ is the first phase to form, being thermally stable up to 310 °C and exhibiting ferromagnetic properties up to $T_C \sim 300$ K.

Introduction

The Mn-Ge system is highly regarded for integration of spintronic applications in the Complementary Metal Oxide Semiconductor (CMOS) technology based on Si and Ge materials. Two main routes are currently investigated: i) the possibility to create a Mn-doped Ge diluted magnetic semiconductor (DMS) exhibiting tunable magnetic properties due to the use of electric field, and (ii) the fabrication of a ferromagnetic Mn₅Ge₃ layer in epitaxy on Ge(111), which could be used as an electric contact for spin injection in monocrystalline Ge without the use of a tunnel barrier. Understanding Mn incorporation in Ge bulk is of great interest for DMS fabrication. Substitutional Mn atoms are double acceptors, promoting *p*-type doped Ge, while interstitial Mn atoms are donors that compensate both holes and magnetic moments due to substitutional Mn [1-2]. However, the Mn solubility limit in Ge is not really known (vary from 0.2 to 6 % in the literature [2-3]). In addition, the proportion of substitutional Mn versus interstitial Mn is still under debate, and the charge of substitutional Mn ions is not clear: Mn atoms can have different positive or negative charge states in Ge [1-2]. Mn diffusion experiments can provide valuable information concerning Mn incorporation in Ge: the Mn diffusion profiles inform about the Mn solubility limit (only mobile Mn atoms are in solution), and the knowledge of the Mn diffusion mechanism in Ge should help to determine the proportion of substitutional and interstitial Mn atoms incorporated in Ge, and inform on Mn-point defects pairing. Since Mn is a dopant element for Ge, the diffusion of high concentration Mn can allow the charge of the Mn atoms to be determined. Of course, the knowledge of the Mn diffusion coefficient is also important for the design of processes allowing for the elaboration of Mn:Ge structures. The Mn₅Ge₃ compound is ferromagnetic, exhibiting a relatively high Curie temperature (T_C) close to room temperature, with the possibility of increasing

it up to 450 K using C or Fe doping [4-5]. In addition, thin Mn_5Ge_3 films can be grown in epitaxy on Ge(111) and can present high spin polarization [6-7]. This is why spin current injection from Mn_5Ge_3 to Ge is expected to be performed at room temperature, without the use of a tunnel barrier between Mn_5Ge_3 and Ge(111). However, it is important to be able to control the formation of the phase Mn_5Ge_3 , preventing the others undesired Mn-Ge compounds to form, and to be sure that the Mn_5Ge_3 layer will not be damaged by the several process steps of device fabrication (phase stability). The self-aligned silicide (Salicide) process is widely used in CMOS technology to produce ohmic contacts on Si [8]. It is based on the reaction between a metallic thin-film and the Si substrate [9]. This process should be also applied to the fabrication of Mn_5Ge_3 contacts on Ge. Thus, it is crucial to understand solid state reaction between a thin Mn film and a Ge substrate.

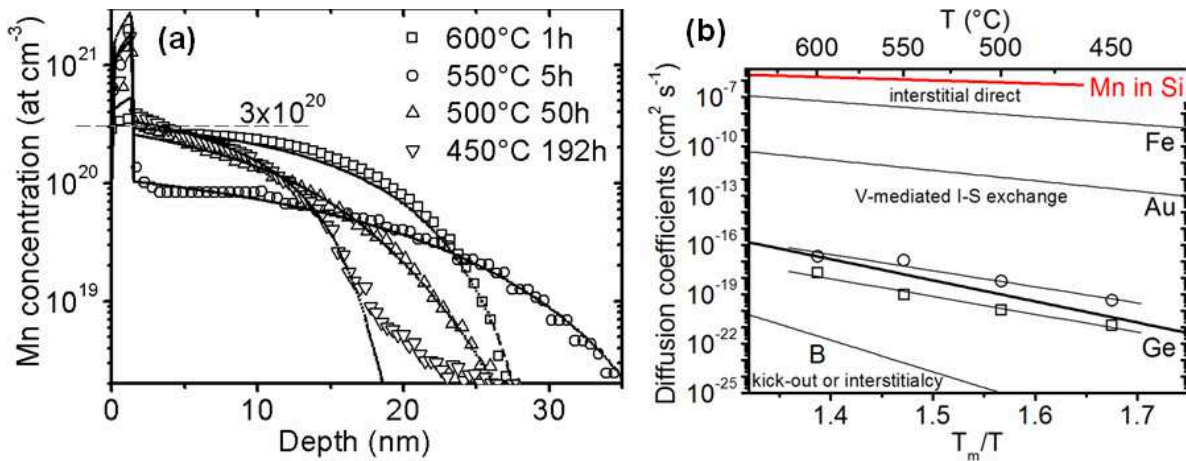


Fig. 1. (a) Mn concentration profiles measured by SIMS after different annealing (open symbols) and the corresponding simulation profiles (solid lines) allowing the Mn diffusion coefficients to be determined; (b) Mn diffusion coefficients measured in the present study (open circles for uncharged defects D_0 , open squares for charged defects D_I) compared with diffusion coefficients of other species (Ge [17], Fe [18], Au [19] and B [20]) in Ge. The Mn diffusion coefficient in Si [21] is also given (red thick solid line). Coefficients are given versus the ratio T_m/T , with T_m the melting temperature of the considered matrix (Ge or Si).

Mn diffusion in Ge: Ge(Mn) DMS

For the Mn diffusion experiments in Ge, a Sb-doped Ge(001) substrate with a resistivity of $0.34 \Omega \text{ cm}$ was loaded in a commercial molecular beam epitaxy (MBE) chamber exhibiting a base pressure $P \sim 1 \times 10^{-10}$ Torr, and equipped with standard Mn and Ge effusion cells [10]. The substrate was annealed several hours at a temperature $T = 450 \text{ }^\circ\text{C}$ before to be heated up to $750 \text{ }^\circ\text{C}$ for few seconds in order to obtain a clean Ge surface. Once back to room temperature, 0.5 atomic monolayer (ML) of Mn was deposited on the Ge substrate. The sample was then annealed in situ in the MBE at $250 \text{ }^\circ\text{C}$ for three hours in order to form the initial Mn diffusion source close to the sample surface. Thus, the sample was cut into $1 \times 1 \text{ cm}^2$ pieces and each of the sample pieces were annealed separately in a furnace under vacuum ($P < 7.5 \times 10^{-8}$ Torr) at different T (from 450 to $750 \text{ }^\circ\text{C}$) and for different times t . Mn concentration profiles were measured by secondary ion mass spectrometry (SIMS) using an ADEPT 1010 Dynamic SIMS system operated at 2 kV with an O^{2+} primary ion beam with an impact angle of 40° compared with the normal of the sample surface. The samples' surface was studied by Auger electron spectroscopy (AES) and atomic force microscopy (AFM) in air, while the magnetic properties of the samples were studied by electron spin resonance (ESR) [11]. Fig. 1a presents the SIMS profiles measured in the samples after four different annealing from $450 \text{ }^\circ\text{C}$ to $600 \text{ }^\circ\text{C}$. Annealing at higher temperatures led to Mn evaporation from the sample surface and no diffusion profile could be measured in the samples [10]. The simulation that allowed the Mn lattice diffusion coefficient to be measured are also shown (solid lines) in the same figure. The diffusion profiles could be simulated considering Mn atoms to be entirely activated on

Ge lattice substitutional sites carrying a negative charge. Since Mn atoms are known to be double acceptors, the configuration Mn^{2-} was chosen. Eq. 1 gives the expression of the atomic flux (J) considering the internal electric field due to the interactions between the Mn^{2-} ions and the delocalized holes. D_{eff} is the Mn effective diffusion coefficient, $q = -2$ is the (elementary) charge carried by the Mn ions and $a = C^2 + 4|q|n_i^2$ with C the Mn concentration and n_i the intrinsic electron concentration [10]. Eq. 2 describes how the Mn diffusion coefficient varies with charged defect concentration: D_0 corresponds to the Mn diffusion coefficient mediated by uncharged point defects for which the concentration is independent of the Ge Fermi level, D_I corresponds to the diffusion coefficient mediated by charged point defects for which the concentration varies with the Fermi level, and h is the local concentration of holes. In addition to these usual equations for dopant diffusion in semiconductors, it was necessary to take into account in the diffusion equation (Eq. 3) the dissolution of Mn-Ge clusters located on the surface: in eq. 3 k_{cl} is the dissolution rate of the clusters, and C_{cl} the concentration of Mn atoms in the clusters. The presence of Mn-Ge clusters on the sample surface was confirmed by AES [10] and AFM measurements (Fig. 2b).

$$J = -D_{eff} \left(1 + \frac{|q|C}{\sqrt{a}} \right) \frac{dC}{dx} \quad (1)$$

$$D_{eff} = D_0 + D_I \frac{h}{n_i} \quad (2)$$

$$\frac{dC}{dt} = -\frac{dJ}{dx} + k_{cl}C_{cl} \quad (3)$$

Fig. 1b presents the Mn diffusion coefficients we measured using Eqs. 1, 2, and 3, compared to the diffusivity of other elements using different diffusion mechanisms in Ge. We found $D_0 = 1.54 \cdot 10^{-3} \exp(-2.36 \text{ eV}/kT) \text{ cm}^2 \text{ s}^{-1}$ and $D_I = 1.29 \cdot 10^{-3} \exp(-2.60 \text{ eV}/kT) \text{ cm}^2 \text{ s}^{-1}$. C_{cl} was found to correspond to Mn concentrations higher than a solubility limit of $4 \times 10^{20} \text{ cm}^{-3}$, and k_{cl} was found to vary from $1.55 \times 10^{-6} \text{ s}^{-1}$ at $450 \text{ }^\circ\text{C}$ to $7.7 \times 10^{-4} \text{ s}^{-1}$ at $600 \text{ }^\circ\text{C}$, following the Arrhenius law $k_{cl} = 6.43 \times 10^8 \exp(-2.13 \pm 0.01 \text{ eV}/kT) \text{ s}^{-1}$. As can be seen in Fig. 1b, the Mn diffusivity is close to the Ge one, indicating that Mn diffusion is probably vacancy mediated. In addition, the Mn solubility limit for $450 \leq T \leq 600 \text{ }^\circ\text{C}$ was found to be 0.7-0.9 at % (corresponding to $3\text{-}4 \times 10^{20} \text{ cm}^{-3}$, see Fig. 1a). In these samples, all the Mn atoms are dissolved on substitutional sites and no clusters have been formed in the Ge bulk due to the use of the equilibrium diffusion process to incorporate Mn in Ge. Thus, ideal Ge(Mn) solutions have been fabricated. Fig. 2a presents ESR measurements (black solid line) performed on the sample annealed at $500 \text{ }^\circ\text{C}$ for 50 hours (Fig. 1a).

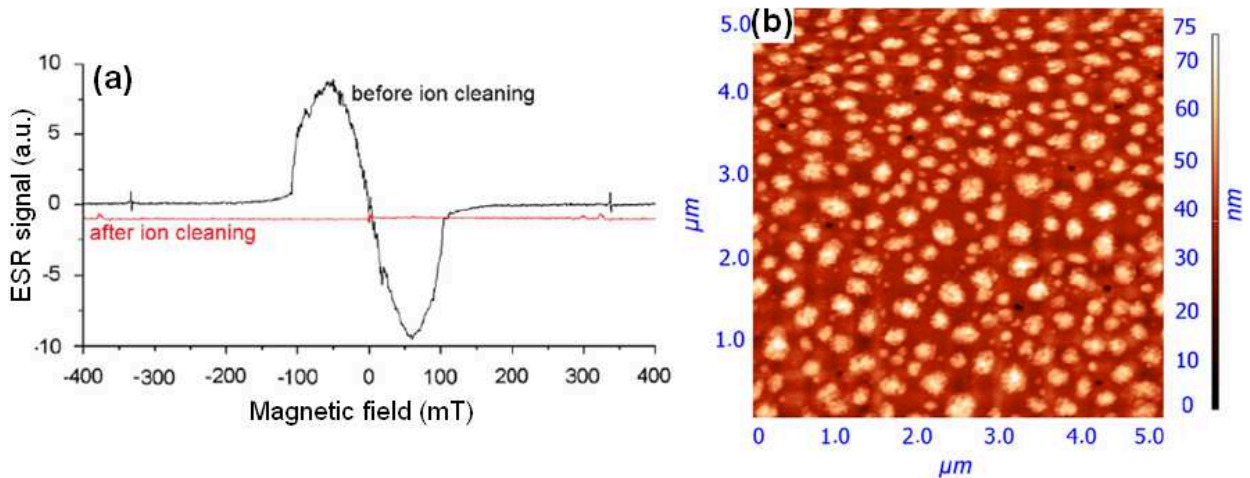


Fig. 2. (a) ESR signal versus magnetic field intensity measured in the same Ge(Mn) sample before (black solid line) and after (red solid line) Ar^+ ion bombardment of the surface; and (b) AFM in air measurements performed on the sample surface before Ar^+ ion bombardment.

A broad signal appears at zero magnetic field that is typical to a ferromagnetic spectrum at microwave frequency lower than the anisotropic gap, and that could correspond to a Ge(Mn) DMS. However, due to the presence of Mn-Ge islands on the surface (Fig. 2b) that could also be the origin of the ferromagnetism, the sample was loaded in an ultra high vacuum chamber equipped with AES and with an Ar⁺ ion gun, and the islands were removed from the surface by Ar⁺ ion bombardment [11]. In situ AES and ex situ AFM confirmed that no Mn and no island was present on the surface after ion bombardment, and SIMS measurements were used to check that despite the surface cleaning, enough Mn atoms were still present in the sample bulk to be detected by ESR after ion bombardment [11]. Fig. 2a shows the results of ESR measurements performed on the same sample after bombardment (red solid line). The initial ferromagnetic signal has vanished after the surface cleaning. Consequently, the ferromagnetic signal was due to the Mn-Ge clusters formed on the Ge surface. The only signal detected by ESR was the paramagnetic signal of substitutional Sb atoms corresponding to the Ge substrate doping background [11]. No signal could be detected from Mn atoms, in agreement with Mn atoms being dissolved on Ge substitutional sites in an ion electronic configuration different from Mn¹⁺ [12], probably in the configuration Mn²⁺. Substitutional Mn atoms are not ferromagnetic in Ge, and thus, the production of a Ge(Mn) diluted magnetic semiconductor is not possible.

Mn-Ge reactive diffusion: spin injection through Mn₅Ge₃

In order to study Mn/Ge solid state reactive diffusion, a 50 nm-thick polycrystalline Mn layer was deposited on a 150 nm-thick amorphous Ge (a-Ge) layer deposited on a thermally oxidized silicon wafer (120 nm-thick SiO₂/Si(100) substrate) using electron beam evaporation under vacuum (base pressure $P \sim 4 \times 10^{-9}$ Torr). Mn and Ge depositions were sequentially performed in the same chamber at room temperature. Reaction between Mn and Ge was studied using in situ XRD measurements performed under vacuum ($P \sim 5 \times 10^{-6}$ Torr) in the Bragg-Brentano geometry: the samples were brought to 100 °C before to be annealed following a temperature ramp of 5 °C/min. The samples' microstructure was studied by transmission electron microscopy (TEM), and their magnetic properties were investigated using a superconducting quantum interference device (SQUID) [13]. The atomic distribution in the crystallized Ge substrate was analyzed in three dimensions at the atomic scale by laser-pulsed atom probe tomography (LP-APT) at $T = 30$ K using a laser power ~ 0.8 nJ [14]. Fig. 3a presents the diffractogram variations versus annealing temperature. Two phases appear sequentially. The first phase's diffraction peaks correspond to the (210), (211), and (112) planes of the Mn₅Ge₃ compound (solid squares in Fig. 3a), and the second phase's diffraction peaks correspond to the (311), (106), (107), (421), (704), and (327) planes of the Mn₁₁Ge₈ compound (solid circles in Fig. 3a). Two Mn-rich phases are missing in the sequence: Mn_{3,4}Ge (77 Mn at %) and Mn₇Ge₃ (70 Mn at %). In addition, some of the diffraction peaks corresponding to Mn₁₁Ge₈ correspond also to Ge (open squares in Fig. 3a). Their intensity variations indicate that a-Ge crystallizes at 280 °C instead of 570 °C, probably due to metal-induced crystallization [13]. In situ annealing can be stopped at any time to perform ex situ measurements. If the annealing ramp is stopped at 300 °C, the Mn layer has been entirely consumed and the sample contains only the first phase. This phase was confirmed to be Mn₅Ge₃ by high-resolution (HR) TEM and by SQUID, being ferromagnetic with $T_C \sim 297$ K as expected for Mn₅Ge₃ [13]. At the end of the annealing ramp (up to 650 °C) Mn₅Ge₃ has been entirely consumed and the sample contains only the second phase, which was confirmed to be Mn₁₁Ge₈ by HR-TEM and by SQUID [13]. SQUID measurements showed an antiferromagnetic-ferromagnetic transition at $T_{Neel} \sim 141$ K as expected for Mn₁₁Ge₈. However, these measurements showed also the presence in the sample of an unidentified ferromagnetic phase with $T_C \sim 43.5$ K. This phase could not be detected by XRD and HR-TEM. Consequently, this ferromagnetic phase is expected to be related to either the formation of a Ge(Mn) DMS thanks to Mn diffusion in the Ge substrate during annealing, or to very small clusters or precipitates. Fig. 3b shows a cross-sectional TEM image obtained after stopping the annealing ramp at 350 °C. At that stage, XRD measurements show the coexistence of Mn₅Ge₃ and Mn₁₁Ge₈ with crystallized Ge. This scenario is confirmed by TEM: one can observe the three-layers

stack $\text{Mn}_5\text{Ge}_3/\text{Mn}_{11}\text{Ge}_8/\text{poly-Ge}$ on the $\text{SiO}_2/\text{Si}(001)$ substrate. This image confirms the sequential growth regime of phases, since $\text{Mn}_{11}\text{Ge}_8$ has nucleated between Ge and Mn_5Ge_3 once Mn has been totally consumed, as well as the crystallization of Ge (poly-Ge). These results show that the phase formation sequence during Mn(thin-film)/Ge reactive diffusion is Mn/Ge \rightarrow Mn/ $\text{Mn}_5\text{Ge}_3/\text{Ge}$ \rightarrow $\text{Mn}_5\text{Ge}_3/\text{Ge}$ \rightarrow $\text{Mn}_5\text{Ge}_3/\text{Mn}_{11}\text{Ge}_8/\text{Ge}$ \rightarrow $\text{Mn}_{11}\text{Ge}_8/\text{Ge}$. In addition, the Mn_5Ge_3 nano-layer is found to be stable up to 310 °C. In order to identify the ferromagnetic phase exhibiting $T_C \sim 43.5$ K at the end of the annealing ramp, LP-APT measurements were performed in the poly-Ge substrate. Fig. 3c presents two images of a same volume ($30 \times 30 \times 120 \text{ nm}^3$) in the poly-Ge substrate analyzed by LP-APT. Each single point is a single atom of the volume. For clarity, only 50 % of all the detected Ge atoms (red) are presented with 100 % of the detected O atoms (blue) in the first image, while only the Mn atoms (purple) are presented in the second image. The O atoms correspond to the SiO_2 layer at the poly-Ge/ SiO_2 interface (Fig. 3b). The APT analyses showed that the distribution of Mn atoms in poly-Ge is not homogeneous (Fig. 3c) since Mn atoms are mainly located in Ge grain boundaries (GBs) and triple junctions (TJs) (fast diffusing path [15-16]). No Mn atoms could be detected in Ge grains ($< 10^{-19}$ at cm^{-3}), meaning that Mn atoms did not diffuse in Ge grains to form a Ge(Mn) DMS. However, LP-APT measurements showed that very small Mn-Ge and Mn-Ge-C clusters have been formed in GBs and TJs (Fig. 3c). These clusters exhibit a diameter smaller than 4 nm and contain a Mn concentration lower than 6 %. Comparing XRD, HR-TEM and HR-LP-APT analyses, these clusters appear to be the only additional phase that can exhibit ferromagnetic properties.

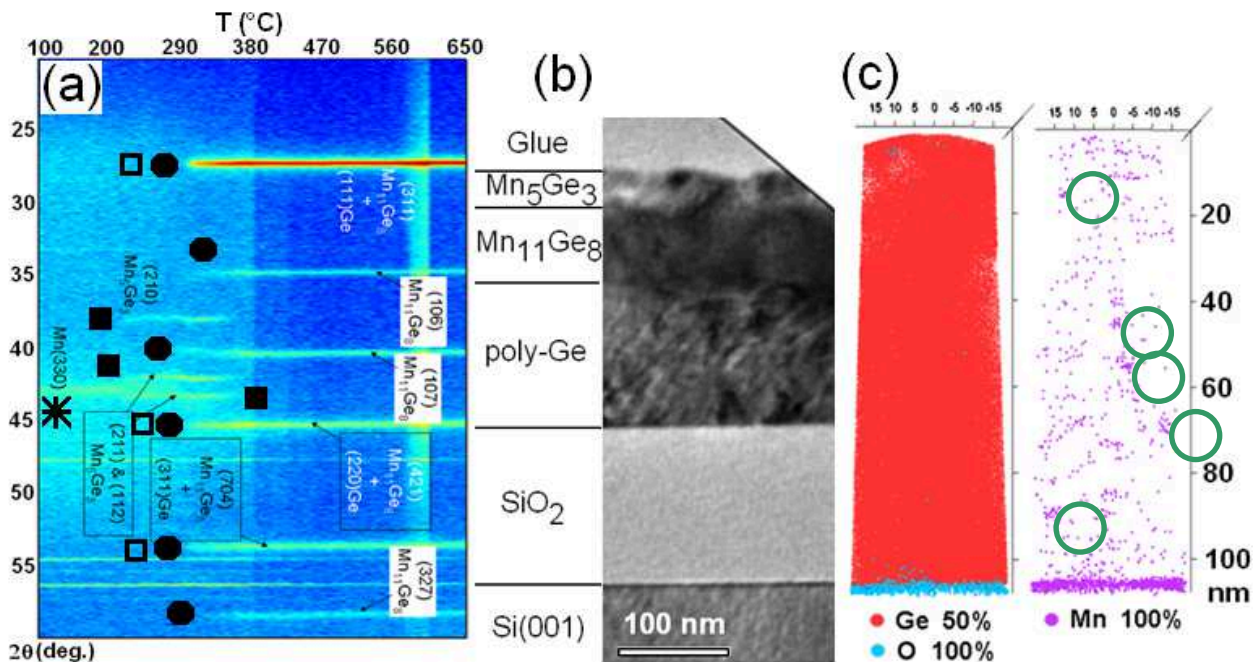


Fig. 3. (a) in situ XRD measurements: the diffraction angle 2θ is given versus the ramp temperature (star for Mn, solid squares for Mn_5Ge_3 , solid circles for $\text{Mn}_{11}\text{Ge}_8$, and open squares for Ge); (b) TEM cross-sectional image for annealing stopped at 350 °C; and (c) APT volume ($30 \times 30 \times 120 \text{ nm}^3$) measured in poly-Ge after the end of annealing up to 650 °C, the green circles highlights some of the Mn clusters.

Summary

The formation of a Ge(Mn) solution by solid state diffusion for DMS fabrication, as well as the Mn/Ge reactive diffusion for spin-injector contact fabrication on Ge have been investigated. The Mn lattice diffusion coefficient in Ge has been measured, and the Mn solubility in Ge was found to be $\sim 0.7\text{-}0.9\%$ ($450 \leq T \leq 600^\circ\text{C}$). Mn atoms are dissolved on Ge substitutional sites, probably in the Mn^{2+} ion configuration, and substitutional Mn atoms are not ferromagnetic in Ge. Ge(Mn) DMS cannot be produced, and concentrated Ge(Mn) solutions are expected to contain Mn-Ge clusters due to the low Mn solubility in Ge. Actually, ferromagnetic signals usually attributed to Ge(Mn) DMS

are probably related to surface or bulk Mn-Ge and Mn-Ge-C nano-clusters containing a low concentration of Mn (different stoichiometry from Mn_5Ge_3 : unstable clusters before Mn_5Ge_3 nucleation). Mn(thin-film)/Ge reaction leads to the sequential growth of the Mn_5Ge_3 and $\text{Mn}_{11}\text{Ge}_8$ compounds. Mn_5Ge_3 is thus the first phase to form. It exhibits ferromagnetic properties up to $T_C \sim 300$ K and it is thermally stable up to 310°C . Thus, the Salicide process appears as a potential method for Mn_5Ge_3 nano-layer fabrication on Ge for spintronic applications. The phase of interest is forming first, however, the thermal stability of Mn_5Ge_3 needs to be increased (as it has been done for NiSi) in order to be used in realistic industrial processes.

References

- [1] S.J. Pearton: Solid-State Electronics Vol. 25 (1982) 499.
- [2] M.C. Dolph, T. Kim, W. Yin, D. Recht, W. Fan, J. Yu, M.J. Aziz, J. Lu, S.A. Wolf: J. Appl. Phys. Vol. 109 (2011) 093917.
- [3] J.-P. Ayoub, L. Favre, I. Berbezier, A. Ronda, L. Morresi, N. Pinto, Appl. Phys. Lett. Vol. 91 (2007) 141920.
- [4] Y. Tawara and K. Sato: J. Phys. Soc. Jpn. Vol. 18 (1963) 773.
- [5] A. Spiesser, M.-T. Dau, L. A. Michez, M. Petit, C. Coudreau, A. Glachant, V. Le Thanh: Int. J. Nanotechnol. Vol. 9 (2012) 428.
- [6] S. Olive-Mendez, A. Spiesser, L.A. Michez, V. Le Thanh, A. Glachant, J. Derrien, T. Devillers, A. Barski, M. Jamet: Thin Solid Films Vol. 517 (2008) 191.
- [7] R.P. Panguluri, C. Zeng, H.H. Weitering, J.M. Sullivan, S.C. Erwin, B. Nadgorny: Phys. Status Solidi B Vol. 242 (2005) R67.
- [8] K. Hoummada, I. Blum, D. Mangelinck, A. Portavoce: Appl. Phys. Lett. Vol. 96 (2010) 261904.
- [9] P. Gas, C. Girardeaux, D. Mangelinck, A. Portavoce: Mat. Sci. Eng. B Vol. 101 (2003) 43.
- [10] A. Portavoce, O. Abbes, Y. Rudzevich, L. Chow, V. Le Thanh, C. Girardeaux: Scripta Materialia Vol. 67 (2012) 269.
- [11] A. Portavoce, S. Bertaina, O. Abbes, L. Chow, V. Le Thanh: Mat. Lett. Vol. 119 (2014) 68.
- [12] G. Ludwig and H. Woodbury: Phys. Rev. Vol. 113 (1959) 1014.
- [13] O. Abbes, A. Portavoce, V. Le Thanh, C. Girardeaux, L. Michez: Appl. Phys. Lett. Vol. 103 (2013) 172405.
- [14] O. Abbes, Ph.D. Thesis, Aix-Marseille University, 2013.
- [15] A. Portavoce, G. Chai, L. Chow, J. Bernardini: J. Appl. Phys. Vol. 104 (2008) 104910.
- [16] A. Portavoce, L. Chow, J. Bernardini: Appl. Phys. Lett. Vol. 96 (2010) 214102.
- [17] M. Werner, H. Mehrer, H.D. Hochheimer: Phys. Rev. B Vol. 32 (1985) 3930.
- [18] A.A. Bugai, V.E. Kosenko, E.G. Miselyuk: Sov. Phys. Tech. Phys. (English Transl.) Vol. 2 (1957) 183.
- [19] H. Bracht, N.A. Stolwijk, H. Mehrer: Phys. Rev. B Vol. 43 (1991) 14465.
- [20] S. Uppal, A.F.W. Willoughby, J.M. Bonar, N.E.B. Cowern, T. Grasby, R.J.H. Morris, M.G. Dowsett: J. Appl. Phys. Vol. 96 (2004) 1376.
- [21] D. Gilles, W. Bergholz, W. Schröter: J. Appl. Phys. Vol. 59 (1986) 3590.